International Journal of Heat and Mass Transfer 103 (2016) 715–724

Contents lists available at ScienceDirect

International Journal of Heat and Mass Transfer

journal homepage: www.elsevier.com/locate/ijhmt

Design of microchannel heat sink with wavy channel and its time-efficient optimization with combined RSM and FVM methods

Jiandong Zhou [a], M. Hatami [a,b], Dongxing Song [a], Dengwei Jing [a,*]

[a] International Research Center for Renewable Energy, State Key Laboratory of Multiphase Flow in Power Engineering, Xi'an Jiaotong University, Xi'an 710049, China
[b] Department of Mechanical Engineering, Esfarayen University of Technology, Esfarayen, North Khorasan, Iran

ARTICLE INFO

Article history:
Received 28 June 2016
Received in revised form 22 July 2016
Accepted 27 July 2016

Keywords:
Heat transfer enhancement
MCHS
Wavy channel
RSM

ABSTRACT

In this study, a sinusoidal wavy structure of microchannel heat sink intended for active cooling of compact electronic devices such as insulated-gate bipolar transistor (IGBT) has been designed. By combining with the finite volume method (FVM), the geometric parameter of the wavy wall, as the key factor to improve the heat transfer efficiency, has been optimized by a novel response surface methodology (RSM), which has found to be time-efficient and accurate. Furthermore, we use a comprehensive heat transfer index β to study whether the heat transfer enhancement outweighs the increased pressure drop. After investigating the *Re*, *h*, ΔP, *f*, β, it is concluded that the best case is occurred when wave amplitude value is 40 and wavelength is 100. For our optimized wavy channel, the heat transfer can be enhanced by a maximum of 2.8 times compared to regular straight channel. CFD simulation demonstrates that under such case, the existence and disturbance of vortex can lead to thinning of boundary layer and hence more effective heat transfer. Our results should have practical value for designing of compact heat exchanger and the proposed optimization method is supposed to have wide application for the time-efficient optimization of heat transfer through irregular configurations.

1. Introduction

Miniaturization and compactness of heat sink for electronic devices are crucial for devices such as PC, mobile phone and even artificial satellite. In order to ensure the working reliability of those electronic instruments with higher power density, even small heat emission problem must be solved. Other than electronic equipment, large machinery such as locomotive traction system also faces difficulty in heat dissipation. For this system, insulated-gate bipolar transistor (IGBT) is its key component unit, which generates a huge amount of heat due to high switching frequency and flow through of huge current. To maintain the temperature of IGBT in safety zone is therefore crucial for its steady and safe operation. For most of such devices, active cooling by air or water are the most commonly methods for dissipating additionally generated heat. Among numerous types of heat exchangers, microchannel heat exchangers have received great attention in recent years as noted in several reviews [1–3]. For instance, recent development of microchannel heat sink (MCHS) was summarized by Smakulski et al. [4]. An elaborate comparison on the technology, operating fluids, flow character, heat transfer coefficient, pressure drop, Reynolds number and the media type, etc., were present in this review. Tuckerman and Pease [5] are among the pioneering researchers in applying the concept of microchannel heat sink with forced convection. They designed a new compact, water-cooled integral heat sink with microchannel and found that it showed an excellent efficiency of heat exchange. Generally, microchannel heat exchangers are composed by a lot of parallel microchannels with a hydraulic diameter ranging from 10 μm to 1000 μm. In such design, the heat exchangers are usually bonded with the heat-dispersing surfaces by heat conduction silica gel. The coolant flows through the microchannels and carries out the needless heat for generating uniform temperature distributions. Recently, the heat transfer and fluid flow processes in rectangular microchannel has been studied by Lee and Garimella [6]. They pointed that conventional analysis approach can be employed in predicting heat transfer behavior in microchannels. However, the entrance and boundary conditions imposed in the experiment need to be carefully matched in the predictive approaches. Tazraei et al. [7,8] investigated the features of fast transient non-Newtonian fluids flow and found that the non-Newtonian behavior of fluids has significant influence on the velocity and shear stress profiles and also on the magnitude of pressure heat and wall shear stress. On the other hand, some researchers designed MCHS with different structures in order to enhance heat transfer performance. Cui et al. [9]

* Corresponding author.
E-mail address: dwjing@mail.xjtu.edu.cn (D. Jing).

http://dx.doi.org/10.1016/j.ijheatmasstransfer.2016.07.100
0017-9310/

investigated the characteristics of fluid flow and heat transfer in a novel microchannel heat sink with triangular cavities and rectangular ribs (TC-RR). The results showed that TC-RR microchannel significantly enhanced heat transfer efficiency due to the interruption and redevelopment of thermal boundary layer. Xia et al. [10] studied the effects of geometric parameters on water flow and heat transfer characteristics in microchannel heat sink with triangular reentrant cavities by numerical simulation method. By comparing four different geometries of the triangular reentrant cavity, they found that the vortices in the triangular reentrant cavities could lead to chaotic advection which dramatically enhanced the convective fluid mixing.

Kim et al. [11] studied the heat transfer enhancement by cross-cut induced flow control in a wavy fin heat exchanger. Parametric study was conducted to find the optimal position and length of the cross-cut. The results showed that heat transfer performance of optimized cross-cut applied plain fin could be enhanced by 23.81% compared to a typical wavy fin. Sabaghan et al. [12] simulated the heat exchange rates in a rectangular microchannel consisting of six longitudinal vortex generators (LVG) based on the two-phase approach. Besides, they also used the nanofluids as the coolant. It was demonstrated that the maximum normalized efficiency of the LVG-enhanced microchannel, compared to the plain channel, could be enhanced by around 14%. There are also many research works about the heat transfer in the microchannel [13–16] carried out by both numerical and experimental methods.

Considering the more and more complicated heat transfer phenomena and/or increased power-density for electron devices in recent years, most of the already existing heat transfer strategies for MCHS become less effective and more efficient MCHSs are apparently highly desired. Therefore, it is still essential to focus on the heat transfer characteristics in microchannel and try to find optimal structures for MCHS that is suitable for certain applications.

Kim et al. [11] have performed simulation using non dimensional governing equations for a steady laminar flow. The parametric study was conducted to find the optimum position and length of the cross-cut wavy fin. Tazraei et al. [17] put forward a novel method, named as the Q_L method, for solving the radiative transfer equation. They also extended the Q_L method to 3D problems in non-grey media and combined it with FVM, ClAM scheme and SLW model to solve the radiative transfer equation. The predictions by this method were found to be accurate and computationally low cost, therefore the results can be used in general code with full reliability. Gorji et al. [18] have investigated the optimal microchannel heat sink geometry by response surface methodology (RSM). They found that RSM can significantly reduce the calculation time and cost. Jafaryar et al. [19] also applied the response surface methodology (RSM) based on central composite design (CCD) to obtain an optimization design for the asymmetric blades geometry of a vertical axis wind turbine (VAWT). In recent studies, Ganji et al. have investigated the finned-tube heat exchangers for diesel exhaust waste heat recovery using CFD and CCD techniques [22]. We have also optimized a circular-wavy cavity filled by nanofluid under the natural convection heat transfer condition by this efficient technique [23].

In our study, taking IGBT as a typical example, we will demonstrate the advantage of RSM for the optimization the wavy microchannel heat sink for heat dissipation of such electronic devices. Specifically, in our work a new 3D heat transfer of wavy MCHS has been designed and compared with rectangular MCHS. In the application of wavy-wall heat transfer systems, an important problem is to determine the optimum geometry. In our study, we will employ the RSM method to optimize the geometry of the microchannel in a time-efficient way. There are two steps to investigate the performance of wavy channel heat transfer. Firstly, we will calculate the Nu, ΔP, τ_w, f values for the convections of wavy walls with different amplitudes and wavelengths under fixed values of *Re*. Then the relationships between convective heat transfer coefficient and the wave amplitude, wavelength, are analyzed. Pressure drop of wavy microchannel of against various wave amplitudes and wavelengths are also analyzed. In the RSM optimization, we will use β as the reference value to find the optimal geometry. By calculating the β under different *Re*, the optimal geometry can be confirmed.

The novelty of our present work compared to previous studied are as follows. Firstly, a sinusoidal wavy structure of microchannel heat sink for potential cooling of electronic devices has been designed. Furthermore, we use a comprehensive heat transfer index β to study whether the heat transfer enhancement outweighs the increased pressure drop. Finally, RSM was combined with the finite volume method (FVM) to find the optimized performance for heat transfer. However, in the previous studies, only single indexes such as Nusselt number or Pressure drop, were used for evaluation of the heat transfer performance.

2. Computational model

2.1. Response surface method (RSM)

Response surface methodology (RSM) is a collection of mathematical and statistical techniques, which was applied to establish a mathematical model between independent variable and dependent variable, and find the effect of parameters affecting a response in a process. The time taken to solve the targeted problem can be reduced and a lot of computation resources are saved by using RSM. Generally, the structure of the relationship between the dependent variable and the independent variables is unknown. The first step in RSM is to find a suitable approximation close to the true relationship. The most common forms are low-order polynomials (first or second order). A second-order model can significantly improve the optimization process when a first-order model suffers from some lack of fit due to the interaction between variables and surface curvatures. A general second-order model is defined as [18]

$$y = a_0 + \sum_{i=1}^{n} a_i x_i + \sum_{i=1}^{n} a_{ii} x_i^2 + \sum_{i=1}^{n}\sum_{j=1}^{n} a_{ij} x_i x_j \big|_{i<j} \quad (1)$$

where x_i and x_j are the design variables, a the tuning parameter and n the number of parameters which is 2 in this case. A Box-Wilson Central Composite Design, also called as a "central composite design" or CCD commonly, is one of options in RSM which helps the user in defining the factor levels.

An imbedded factorial or fractional factorial design is contained in CCD with center points that are augmented with a group of 'star points' which allow an estimation of the curvature. If the distance from the center of the design space to a factorial point is ±1 unit for each factor, the distance from the center of the design space to a star point is $\pm\alpha$ for $|\alpha| > 1$ [20–22]. In the RSM method with CCD, optimization is based on a parameter called 'desirability'. Desirability is an objective function ranging from 0.0 outside of the limits to 1.0 which corresponds to the goal [23]. The numerical optimization finds a point that maximizes the desirability function. The characteristics of the goal may be altered by adjusting the weight or importance. For several responses and factors, all goals get combined into one desirability function. In this study, one response is defined as comprehensive heat transfer index β. The goal of optimization is to find a set of conditions that meet all the goals, instead of to get a desirability value of 1.0. Desirability reflects the preferred ranges for each response (d_i). The simultane-

ous objective function is a geometric mean of all transformed responses:

$$D = (d_1 \times d_2 \times \ldots \times d_n)^{\frac{1}{n}} = \left(\prod_{i=1}^{n} d_i\right)^{\frac{1}{n}} \quad (2)$$

where n is the number of responses in the measurement (in this case, $n = 1$). If any of the responses or factors falls outside their desirability range, the overall function becomes zero. For simultaneous optimization, each response must have a low and high value assigned to each goal. On the CCD worksheet, five option can be chosen in the "Goal" field for responses: "none", "maximum", "minimum", "target", or "in range". In this study, we choose the "maximum" as the goal parameter for comprehensive heat transfer efficiency, as shown below:

$$\begin{aligned} &d_i = 0, \ Y_i \leqslant Low_i \\ &d_i = \left[\frac{Y_i - Low_i}{High_i - Low_i}\right]^{wt_i}, \ Low_i < Y_i < High_i \\ &d_i = 1, \ Y_i \geqslant High_i \end{aligned} \quad (3)$$

where Y_i is the ith response value and wt is the weight of that response. Weight adds emphasis to the goal. In this paper, the weight has a negligible effect on the final results because just one response is defined.

2.2. Straight microchannel heat sink

For comparison, the geometric dimensions of straight microchannel are taken from optimally designed one in literature [24] as show in Table 1. Its bottom size is 28 × 100 mm and the heat flux of 100w/cm² is received from the bottom surface (Fig. 1a). In order to save the computational resources, only one of the straight microchannels is taken as the computational domain as shown in Fig. 1b. In this model, both the two sides of the microchannel contain a half-wall. The geometry parameters of each microchannel are as follows: wall thickness $W_r/2 = 28$ μm; channel width $W_c = 85$ μm; channel height $H_c = 700$ μm and cover plate thickness $H_r = 100$ μm.The rectangular straight microchannel heat sink is used as the benchmark to evaluate the heat transfer performances of wavy channel of various geometries.

2.3. Wavy microchannel heat sink

In this study, single layer wavy microchannel heat sink is initially considered to be an improved design compared to rectangular straight microchannel, as shown in Fig. 1c. All of the dimensions are same as the rectangular straight microchannel other than that straight microchannel becomes wavy. The wave function along x-axis can be determined by,

$$y = A \sin\left(2\pi \cdot \frac{x}{\lambda}\right) \quad (4)$$

where A and λ are defined as amplitude and wavelength, respectively. Also, x is defined as the flow direction.

Table 1
Optimal geometric dimension for straight microchannel heat sink.

L_x (mm)	L_y (μm)	L_z (mm)	W_c(μm)	W_r(μm)	H_c(μm)	$_s$ (μm)	q(W/cm²)
10	900	10	85	56	700	100	100

2.4. Assumption and simplification

In order to simplify the analysis in this study, several assumptions have been made regarding the operating conditions of a wavy channel MCHS.

1. The fluid, which is water in our study, is considered as incompressible laminar flow across a channel and maintains the condition of single phase,
2. We will consider both thermally and hydraulically fully developed flow.
3. The thermophysical properties of the solid are constant.
4. The surface of the MCHS is well insulated.

3. Mathematical modeling

Based on the assumptions above, the governing equations for this model are as follows.

The continuity equation:

$$\frac{\partial u}{\partial x} + \frac{\partial v}{\partial y} + \frac{\partial w}{\partial z} = 0 \quad (5)$$

where u, v, and w are defined as the velocity components in the x, y, and z directions, respectively.

Momentum equations for the coolant:

$$\begin{aligned} \rho_f\left(u\tfrac{\partial u}{\partial x} + v\tfrac{\partial u}{\partial y} + w\tfrac{\partial u}{\partial z}\right) &= -\tfrac{\partial p}{\partial x} + \mu_f(\tfrac{\partial^2 u}{\partial x^2} + \tfrac{\partial^2 u}{\partial y^2} + \tfrac{\partial^2 u}{\partial z^2}) \\ \rho_f\left(u\tfrac{\partial v}{\partial x} + v\tfrac{\partial v}{\partial y} + w\tfrac{\partial v}{\partial z}\right) &= -\tfrac{\partial p}{\partial y} + \mu_f(\tfrac{\partial^2 v}{\partial x^2} + \tfrac{\partial^2 v}{\partial y^2} + \tfrac{\partial^2 v}{\partial z^2}) \\ \rho_f\left(u\tfrac{\partial w}{\partial x} + v\tfrac{\partial w}{\partial y} + w\tfrac{\partial w}{\partial z}\right) &= -\tfrac{\partial p}{\partial z} + \mu_f(\tfrac{\partial^2 w}{\partial x^2} + \tfrac{\partial^2 w}{\partial y^2} + \tfrac{\partial^2 w}{\partial z^2}) \end{aligned} \quad (6)$$

where ρ_f and μ_f are the density and dynamic viscosity of the coolant, respectively, and p is the coolant pressure.

Energy equation for the coolant:

$$\rho_f c_{pf}\left(u\frac{\partial T_f}{\partial x} + v\frac{\partial T_f}{\partial y} + w\frac{\partial T_f}{\partial z}\right) = \kappa_f\left(\frac{\partial^2 T_f}{\partial x^2} + \frac{\partial^2 T_f}{\partial y^2} + \frac{\partial^2 T_f}{\partial z^2}\right) \quad (7)$$

Energy equation for solid region:

$$0 = \kappa_s\left(\frac{\partial^2 T_s}{\partial x^2} + \frac{\partial^2 T_s}{\partial y^2} + \frac{\partial^2 T_s}{\partial z^2}\right) \quad (8)$$

Generally, the thermal properties of water, such as density, viscosity, heat capacity and thermal conductivity, can vary with the temperature change. The expressions of temperature dependent thermophysical properties are given [25] by,

$$\rho(T) = 1000\left[1 - \frac{T + 15.9414}{508929.2(T - 204.87037)}(T - 276.9863)^2\right] \quad (9)$$

$$\mu(T) = 1.005 \times 10^{-3}\left(\frac{T}{293}\right)^{8.9} \mathrm{EXP}[4700(T^{-1} - 293^{-1})] \quad (10)$$

$$k_f(T) = -1.579 + 0.01544T - 3.515 \times 10^{-5}T^2 + 2.678 \times 10^{-8}T^3 \quad (11)$$

The velocity inlet is defined with uniform temperature of 298 K while velocity inlet is specified as 0.6 m/s, 0.8 m/s, 1 m/s, 1.2 m/s, 1.4 m/s, which corresponds to Reynolds number ranges from 99 to 232. The pressure outlet is adopted with atmosphere pressure. Constant heat flux 100 W/cm² is applied at the bottom of MCHS. Symmetrical boundary conditions are assumed on the left and right sides. The boundary conditions are listed as below.

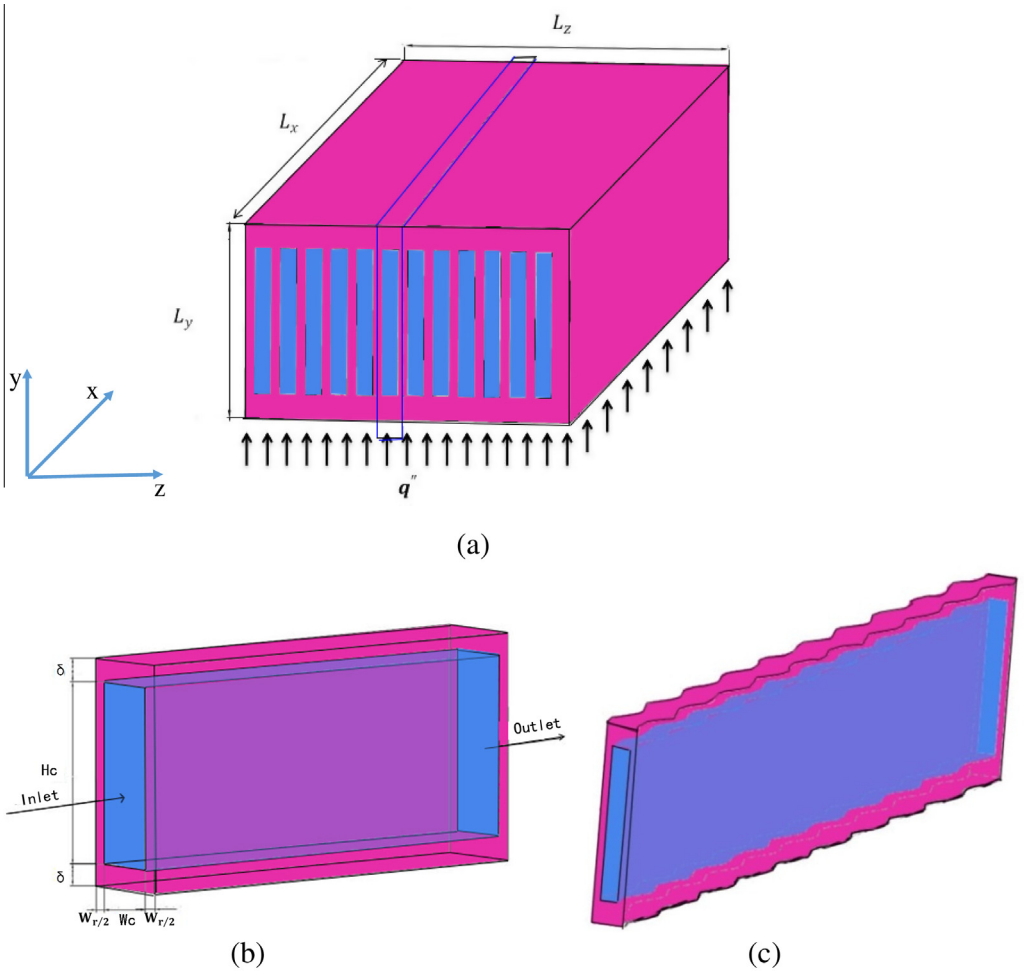

Fig. 1. Schematics of microchannel heat sinks for (a) heat sink, (b) straight microchannel and (c) wavy microchannel. The meanings of all the symbols can be found in Table 1.

Inlet:

$$u = u_{in}, v = 0, w = 0, T = T_{in} \tag{12}$$

Outlet:

$$p = p_{out} \tag{13}$$

Coolant-solid interface:

$$u = 0, v = 0, w = 0, T = T_{in} \tag{14}$$

Bottom wall of the heat sink:

$$q_w = -k_s \frac{\partial T_s}{\partial n} \tag{15}$$

Other solid walls and symmetric boundaries:

$$-k_s \frac{\partial T_s}{\partial n} = 0 \tag{16}$$

Reynolds number is defined as

$$Re = \frac{\rho u_{av} D_h}{\mu} \tag{17}$$

where D_h is the hydraulic diameter defined as $D_h = 2H_c W_{ch}/(H_{ch} + W_{ch})$.

The dimensionless surface heat transfer coefficient, i.e., j factor is defined as,

$$j = \frac{Nu}{Re \cdot Pr^{1/3}} \tag{18}$$

The resistance coefficient is,

$$f = \frac{\Delta P}{\frac{1}{2}\rho u^2} \frac{A}{L} \tag{19}$$

In order to investigate the comprehensive effects of enhanced heat transfer, the comprehensive heat transfer coefficient β is given [26] by

$$\beta = j/f^{1/2} \tag{20}$$

Here β is used to judge whether the increment of heat exchange capability is greater than the increment of flowing resistance at the same pressure drop.

To evaluate the heat transfer characteristics and fluid flow within the wavy channel, finite volume method (FVM) is implemented with the assistance of a CFD commercial package (ANSYS Fluent). The SIMPLEC (semi implicit method for pressure linked equation consisted) algorithm is used to model pressure–velocity coupling. The prescribed convergence criterions of velocities and continuity are 10^{-4}, and for energy, it is set to be 10^{-6}.

4. Results and discussions

4.1. Grid independency test and accuracy of calculation validation

Based on ANSYS Fluent, the 3D conjugate heat transfer problem is numerically solved. As shown in Fig. 2, we use the hexagonal structured grid to deal with geometry, a grid of $1000 \times 104 \times 20$

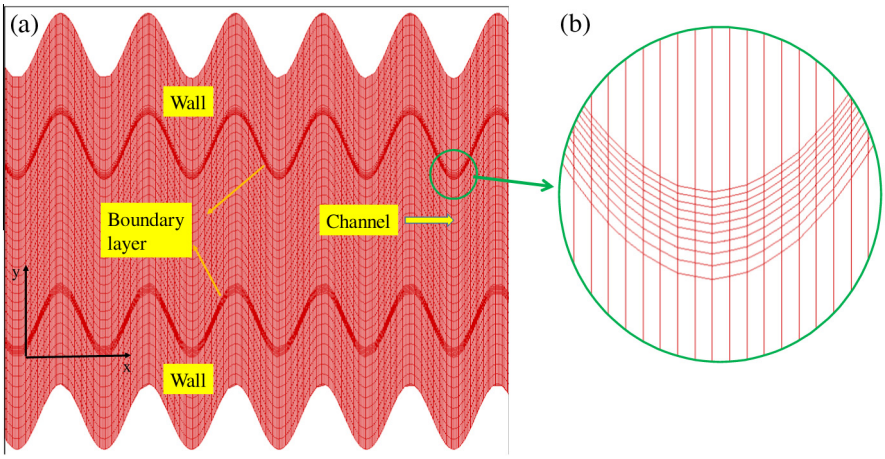

Fig. 2. The computational grids (a) for the calculated domain in the wavy microchannel and (b) the enlarged view near the boundary wall.

was used for the calculation of the flow channel, as shown in Fig. 2 (a). The dense grid cells with successive ratio of 1.2 distribute near the boundaries, as shown in Fig. 2(b) for the enlarged view near the boundary wall. To identify the least mesh-dependence, four mesh numbers of structured grids are considered for grid independence test. The grid independence test is undertaken for the Reynolds number Re = 150 considered in this study, with pure water as coolant inside the microchannel. Fig. 3 shows the results of heat transfer coefficient h calculated over different grid sizes. Since the relative differences of calculated h are less than 0.1% over cell number 4 and 5.5 million, respectively, 5 million cells is deemed appropriate for all the computational simulations carried out in this study.

In order to validate the accuracy of our model, the experimental data of ΔP from the literature [27] were compared with the simulation of our model. The results are depicted in Fig. 4. As can be clearly observed, there is a good agreement between our simulated results and the tendency of the experimental results.

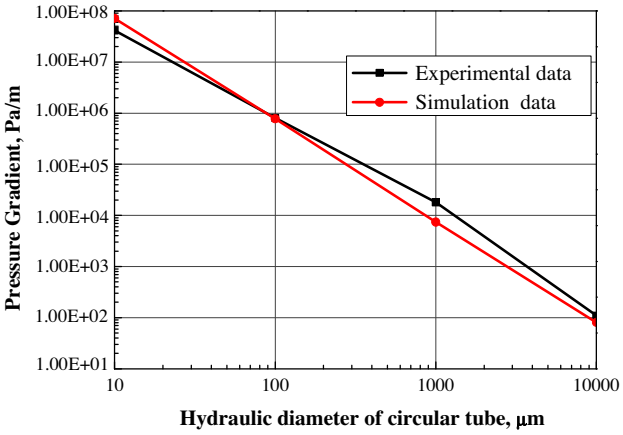

Fig. 4. Validation of the model accuracy with the data available in the literature, S. G. Kandlikar et al. [26].

4.2. The results of CFD simulation

As described, a wavy channel is studied under the laminar flow convective heat transfer. The wall function is $y = A\sin\left(2\pi\cdot\frac{x}{\lambda}\right)$, where A and λ are the wave amplitude and wavelength, respectively. Sakanova et al. [28] considered constant numbers of 25, 50, 75 for A, and 250, 550 for λ, respectively. In this investigation, we want to find optimal constants for these numbers which have a high comprehensive heat transfer coefficient (β). For this aim, CCD is applied for three levels for each of the two factors, A and λ, as shown in Table 2. The wave amplitude A is changed from 10 μm to 40 μm and wavelength λ from 100 μm to 1000 μm. By CCD analysis, 9 different geometries with various amplitudes and wavelength have been studied, as show in Table 2.

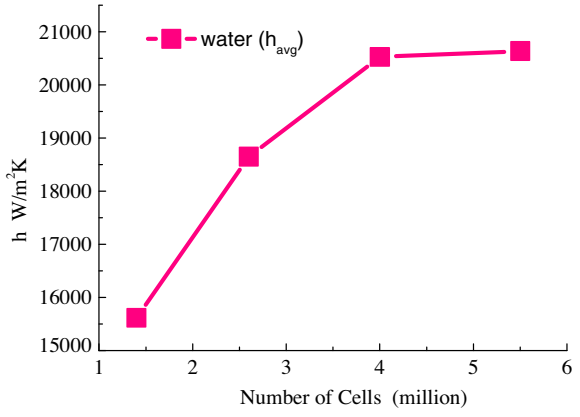

Fig. 3. Grid independency examination for the rectangular microchannel.

Fig. 5 shows the streamlines for nine proposed cases at flow rate u = 1 m/s by the FLUENT. From the streamline contours, it can be observed that the maximum velocity in x direction increases with the increment of wave amplitude at the same wavelength. For instance, the maximum X velocity is shifted from 1.5 m/s to 2.8 m/s when A is adjusted from 10 μm to 40 μm at constant wavelength of λ = 100 μm. In addition, obvious vortex appears in the cases of A = 25, λ = 100 and A = 40, λ = 100. It means that the vortex is more possibly occurred under the larger A and the smaller λ. The

Table 2
Variation of β in different CCD proposed cases when Re = 150.

Case number	A	λ	β
1	10	100	0.046034
2	10	550	0.0422877
3	10	1000	0.0428088
4	25	100	0.0414412
5	25	550	0.0477744
6	25	1000	0.0476693
7	40	100	0.0556904
8	40	550	0.0554782
9	40	1000	0.0417381

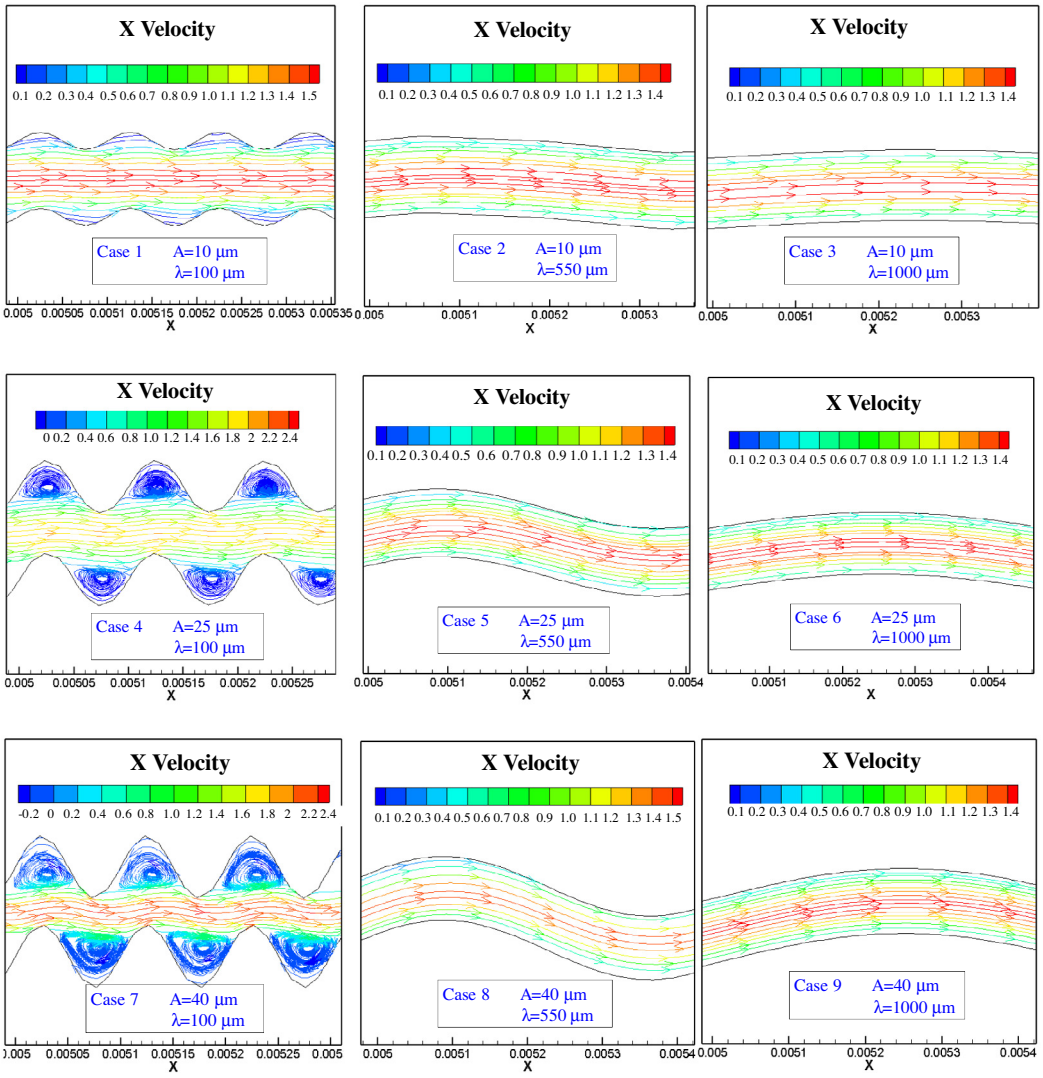

Fig. 5. Velocity vector streamlines along X direction for the typical section of the 9 different geometries of microchannel obtained by RSM.

obtained β values over 9 proposed cases are also given in Table 2. It can be found that the highest and secondly highest heat transfer can be achieved over case 7 and case 8, where vortex can be observed in case 7. The reasons of higher β in case 7 as follows, on the one hand, the higher velocity can accelerate the flow next to wavy peaks, the hydrodynamic and thermal boundary layers are therefore getting thinner. On the other hand, the vortex can cause the disturbance of boundary layer, and make it much thinner. Therefore, there is an increment in heat transfer coefficient for cases such as case 7.

Fig. 6 shows the comparison of wavy-enhanced microchannel with straight microchannel for convective heat transfer coefficient (a) and pressure drop (b), respectively. Fig. 6(a) shows that the relation of convective heat transfer coefficient and Reynolds number. As the *Re* numbers increases, the convective heat transfer coefficient increases. Also, it is obvious that the convective heat transfer coefficient of wavy channels can be significantly improved compare to straight channel. Moreover, it can be seen that for the cases of $A = 40$, $\lambda = 100$; $A = 40$, $\lambda = 550$ and $A = 25$, $\lambda = 100$, they have higher heat transfer coefficients compared to other cases. The results are listed in the size order of h: case 7, case 8, case 4, case 5, case 6, case 1, case 3, case 2, case 9. For example, in the case of $A = 40$ and $\lambda = 100$, the h value is about 2.54 times compared to rectangular channel for low Reynolds number and it becomes 2.81 times with high Reynolds number. From Fig. 6(b), it can be observed that the relation between pressure drop and *Re* number. With the increase of *Re* number, pressure drop increases for all geometries. The variation trends for all the curves are in agreement with the fluid streamlines in Fig. 4. It is apparent that wavy channel has higher pressure drop than rectangular channel. Therefore, it is necessary to investigate the temperature contour and the relationship between h, ΔP and value of wave amplitude, wavelength further.

Fig. 7 presents the temperature contours (K) along X direction for the typical section of the 3 different geometries of microchannel obtained by RSM, which correspond to the normal (case 1), worst (case 4) and optimal (case 7) heat transfer cases, respectively. For all the three cases, one can see that when fluid flows through the channel, both the temperature and the temperature gradients are high near the wall and low in the central region of channel. It can also be found that for case 7, the average temperature is high and also the temperature gradient is quite low. It indicates that geometry of case 7 should be the preferred case in term of heat transfer capacity of the microchannel.

Fig. 8 shows the heat transfer coefficients and pressure drop against *Re* numbers over cases of various wave amplitudes and

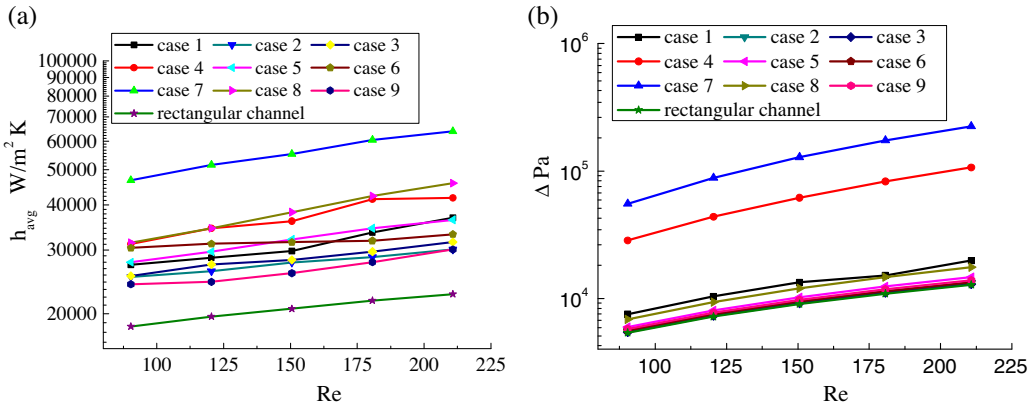

Fig. 6. Comparison of wavy-enhanced microchannel and straight microchannel for convective heat transfer coefficient (a) and pressure drop (b), respectively.

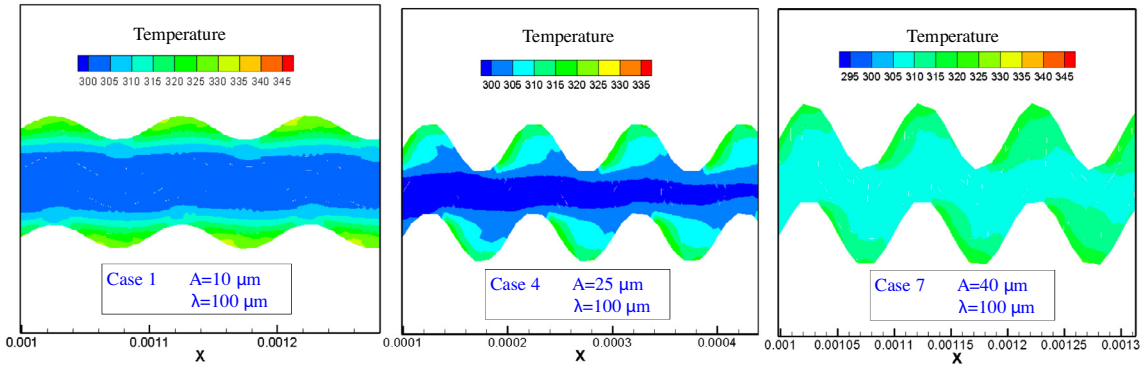

Fig. 7. Temperature contours (K) along X direction corresponding to normal (case 1), worst (case 4) and optimal (case 7) heat transfer cases, respectively.

wavelengths. It can be observed that with the same A and under different λ, the lower the λ of wavy channel, the higher the h and ΔP will be. However, with the same λ and under different A of wavy curved channels, the higher the A of wavy channel, the higher the h and ΔP become. For example, comparing the Figs. 8a–c(1), it has the largest h when $A = 40$ under the same range of wavelength. Also, when $A = 40$, increase of h is much faster than the cases for $A = 10$ and $A = 25$ when λ changes from 100 μm to 1000 μm. Correspondingly, ΔP also shows similar characteristic in Fig. 8a(2)–c(2). What's more, it should be noted that the performance of ΔP shows less difference between $\lambda = 550$ μm and $\lambda = 1000$ μm. Figs. 8d–f show the effect of wavelength on heat transfer and fluid flow. We can see that the same amplitude range with shorter wavelength of wavy channel lead to a higher h and ΔP. Also, it can be observed that the higher the wavelength, the lower the increasing rate of ΔP will be, in the range between $A = 10$ to $A = 40$.

4.3. Optimal design of MCHS by RSM

In order to comprehensively evaluate the performances of heat exchanger, β is defined to judge whether the increment of heat exchange capability is greater than increment of flowing resistance under the same pressure drop, considering the complicated relationships between h and ΔP over various geometrical parameters of wave channels. Table. 2 show the results of RSM analysis of the 9 cases.

Based on the results of RSM analysis from Figs. 6, 8 and 9, a polynomial model with quadratic order is applied for the response (β) and the equation of the β versus A and λ can be found and its contours (2D and 3D) are presented in Fig. 10, which is obtained from DOE software based on CCD analysis. Considering the effects of main factors and also the interactions between the two factors of A and λ, Eq. (1) takes the form,

$$(\beta) = 0.038936 + 8.01987 * 10^{-5}(A) + 2.00901 * 10^{-5}(B) - 3.973 * 10^{-7}(AB) + 7.60548 * 10^{-6}(A^2) - 1.29208 * 10^{-8}(B^2) \quad (21)$$

From the 3D graphs for above formulas as shown in Fig. 8, it can be found that the maximum β occurs in the high A (wave amplitude) and low B (wave length).

As described in Section 2.1 for CCD technique, optimization is based on the desirability with high desirability indicating the better operating condition. Desirability contour for the optimum point can also be found in Fig. 10. One can see that the desirability for the optimal operating point is about 0.927 which corresponds to a good optimization result. The desirability of the selected confirms that the best case (maximum desirability) occurs when $A = 40$ and $\lambda = 100$. In this case, could be as high as 0.0525327. It is therefore chosen as the best case from the comprehensive heat transfer property. To further confirm the accuracy of maximum desirability, all cases of β are investigated in Re numbers ranging from 90 to 210. The results are shown in the Fig. 11. It can be seen that best case for comprehensive heat transfer coefficient β, i.e., $A = 40$ and $\lambda = 100$, is obviously higher than other cases almost over all Re ranges. Also β is found to be decreased with the increase in Re for all cases. It is supposed that with the increment of flow rate, the increase of resistance is quick than heat transfer capacity.

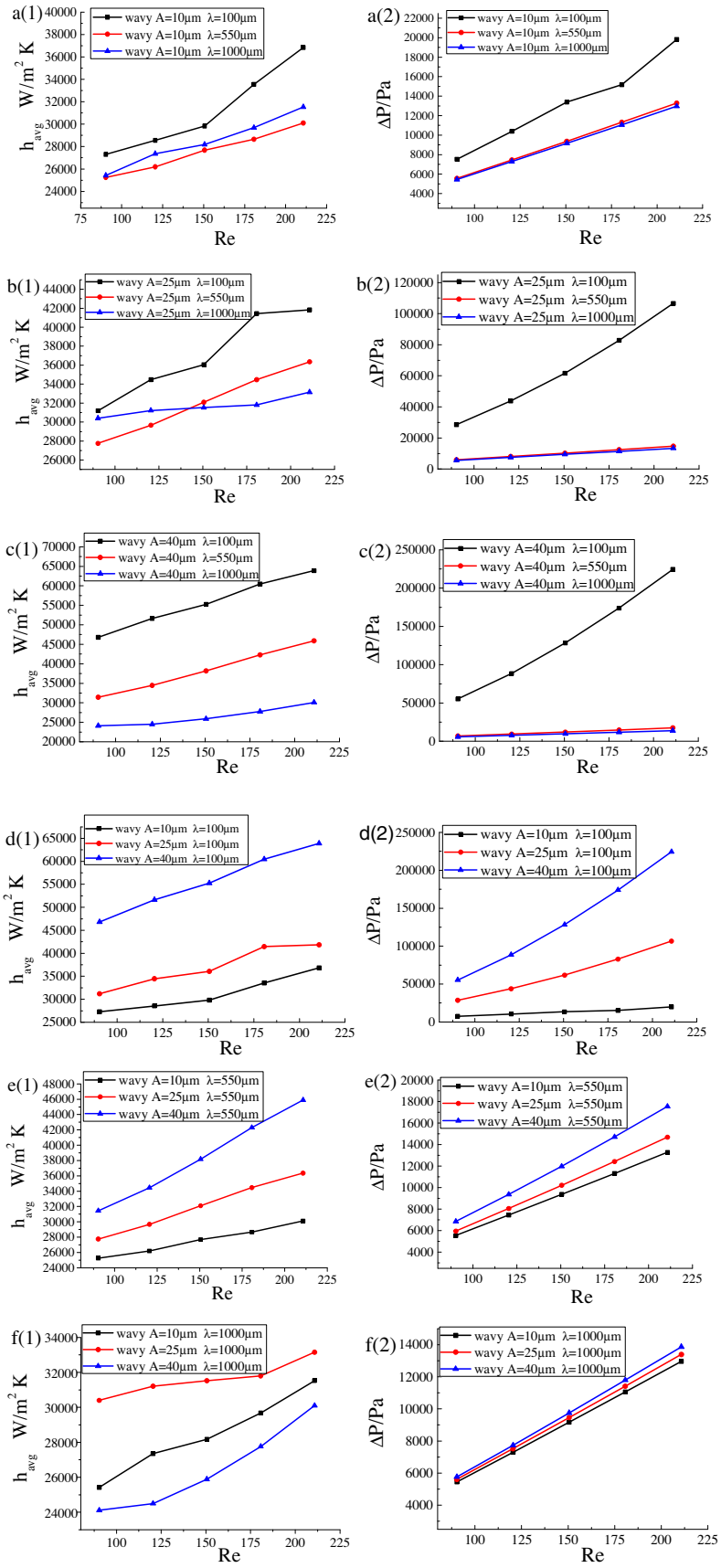

Fig. 8. Heat transfer coefficient and pressure drop at the same amplitude under different wavelength/ at the same wavelength under different amplitude.

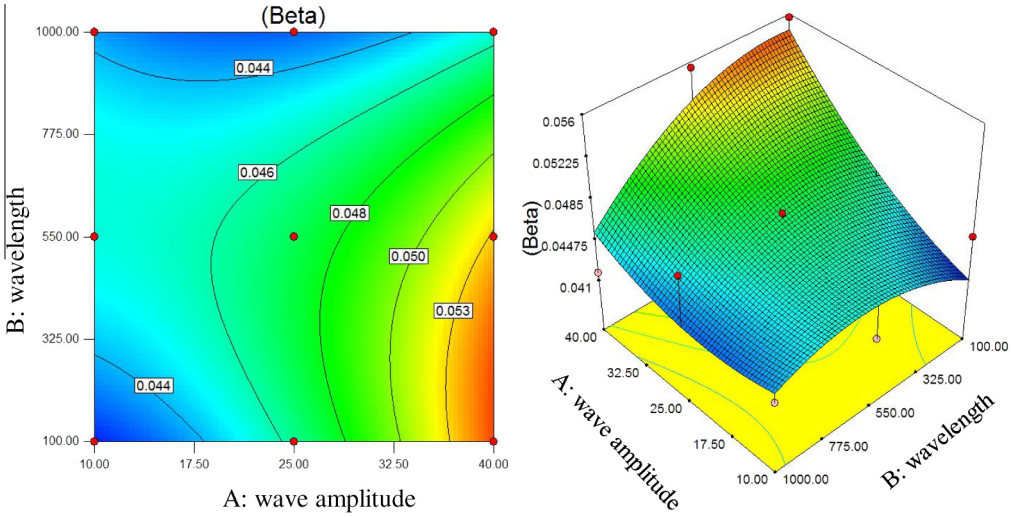

Fig. 9. Effect of A and B parameters on β (a) 2D and (b) 3D.

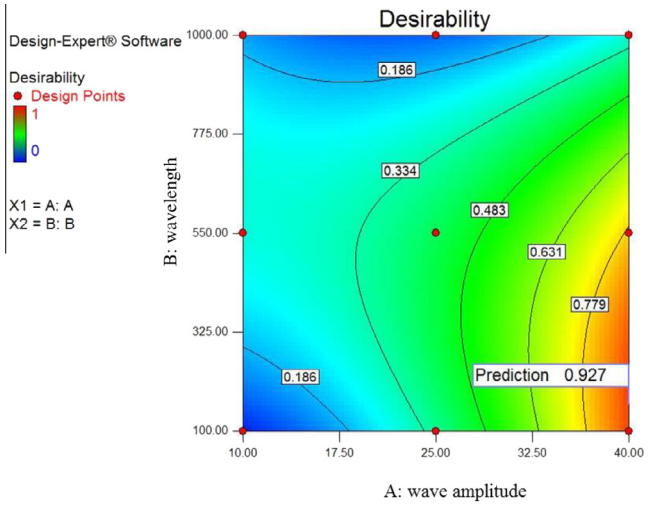

Fig. 10. Desirability contour for the optimum point.

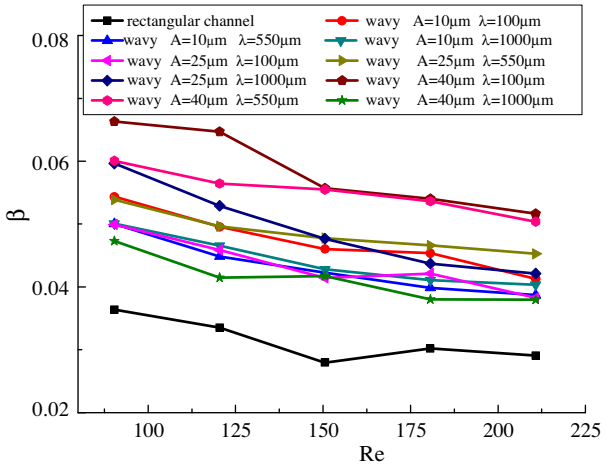

Fig. 11. The comprehensive heat transfer index in 9 cases.

5. Conclusion

In this paper, a new type of MCHS with wavy microchannel structure is put forward. The heat transfer in heat sink is investigated by a numerical method. The effects of wavy amplitude, wavelength, Reynolds number and β are studied. We employed water as the coolant in our design. The results indicate that the heat transfer can be enhanced by a maximum of 2.8 times compared to regular straight channel. It is also found that the higher amplitude and shorter wavelength for wavy channel can lead to a more convective heat transfer coefficient.

In order to obtain the maximum comprehensive heat transfer index β, instead of traditional time-consuming methods, we use RSM to find the optimal geometry for the wavy wall in a time-efficient and accurate way. By combining the RSM and FVM, it is concluded that the best case is when amplitude value is 40 and wavelength is 100. The proposed method, FVM combined with RSM, is supposed to have wide application for the time-efficient optimization of heat transfer through irregular geometry. Moreover, the results of this study are also considered to be of practical value for the optimal designing of active cooling of electronic devices, considering that a small improvement of heat transfer coefficient for these devices is expected to result in great savings in their long-term operation.

Acknowledgments

The authors gratefully acknowledge the financial supports of the National Natural Science Foundation of China (Nos. 51422604, 21276206) and National 863 Program of China (No. 2013AA050402). This work was also supported by the China Fundamental Research Funds for the Central Universities.

References

[1] G. Goss Jr, J.L.G. Oliveira, J.C. Passos, Pressure drop during condensation of R-134a inside parallel microchannels, Int. J. Refrig. 56 (2015) 114–125.
[2] X.W. Yin, W. Wang, V. Patnaik, Evaluation of microchannel condenser characteristics by numerical simulation, Int. J. Refrigeration 54 (2015) 126–141.
[3] J. Zhang, Y.H. Diao, Y.H. Zhao, Y.N. Zhang, An experimental study of the characteristics of fluid flow and heat transfer in the multiport microchannel flat tube, Appl. Therm. Eng. 65 (2014) 209–218.

[4] P. Smakulaki, S. Pietrowicz, A review of the capabilities of high heat flux removal by porous materials, microchannels and spray cooling techniques, Appl. Therm. Eng. (2016).
[5] D.B. Tuckerman, R.F.W. Pease, High-performance heat sinking for VLSI, IEEE Electron Device Lett. 2 (1981) 126–129.
[6] P.S. Lee, S.V. Garimella, D. Liu, Investigation of heat transfer in rectangular microchannels, Int. J. Heat Mass Transfer 48 (2005) 1688–1704.
[7] P. Tazraei, A. Riasi, Quasi-two-dimensional numerical analysis of fast transient flows considering non-Newtonian effects, J. Fluids Eng. 138 (1) (2016) 011203.
[8] P. Tazraei, A. Riasi, B. Takabi, The influence of the non-Newtonian properties of blood on blood hammer through the posterior cerebral artery, Math. Biosci. 264 (2015) 119–127.
[9] G. Xia, Y. Zhai, Z. Cui, Numerical investigation of thermal enhancement in a micro heat sink with fan-shaped reentrant cavities and internal ribs, Appl. Therm. Eng. 58 (2013) 52–60.
[10] G. Xia, L. Chai, H. Wang, Optimum thermal design of microchannel heat sink with triangular reentrant cavities, Appl. Therm. Eng. 31 (2011) 1208–1219.
[11] G.W. Kim, H.M. Lim, G.H. Rhee, Numerical studies of heat transfer enhancement by cross-cut flow control in wavy fin heat exchangers, Int. J. Heat Mass Transfer 96 (2016) 110–117.
[12] A. Sabaghan, M. Edalatpour, M.C. Moghadam, Nanofluid flow and heat transfer in a microchannel with longitudinal vortex generators: two-phase numerical simulation, Appl. Therm. Eng. 100 (2016) 179–189.
[13] L. Chai, G.D. Xia, H.S. Wang, Parametric study on thermal and hydraulic characteristics of laminar flow in microchannel heat sink with fan-shaped ribs on sidewalls – Part 1: heat transfer, Int. J. Heat Mass Transfer 97 (2016) 1069–1080.
[14] P. Li, Y.H. Xie, D. Zhang, Laminar flow and forced convective heat transfer of shear-thinning power-law fluids in dimpled and protruded microchannels, Int. J. Heat Mass Transfer 99 (2016) 372–382.
[15] H.E. Mghari, H. Louahlia-Gualous, Experimental and numerical investigations of local condensation heat transfer in a single square microchannel under variable heat flux, Int. Commun. Heat Mass 71 (2015) 197–207.
[16] G.D. Xia, D. Ma, Y.L. Zhai, Experimental and numerical study of fluid flow and heat transfer characteristics in microchannel heat sink with complex structure, Energy Convers. Manage. 105 (2015) 848–857.
[17] P. Tazraei, The extension of the Q_L method to solve the radiative heat transfer problem in a 3D square enclosure containing non-grey gas, Am. J. Mech. Eng. 4 (2) (2016) 71–81.
[18] M. Rahimi-Gorji, O. Pourmehran, M. Hatami, D.D. Ganji, Statistical optimization of microchannel heat sink (MCHS) geometry cooled by different nanofluids using RSM analysis, Eur. Phys. J. Plus 130 (2015) 1–21.
[19] M. Jafaryar, R. Kamrani, M. Gorji-Bandpy, M. Hatami, D.D. Ganji, Numerical optimization of the asymmetric blades mounted on a vertical axis cross-flow wind turbine, Int. Commun. Heat Mass 70 (2015) 93–104.
[20] W. Kalaoka, S. Witayangkurn, Numerical simulation of natural convection in a partially cooled square enclosure filled with porous medium, Int. J. Pure Appl. Math. 96 (2014) 507–522.
[21] G.A. Florides, P. Christodoulides, P. Pouloupatis, An analysis of heat flow through aborehole heat exchanger validated model, Appl. Energy 92 (2012) 523–533.
[22] M. Hatami, M. Jafaryar, D.D. Ganji, M. Gorji-Bandpy, Optimization of finned-tube heat exchangers for diesel exhaust waste heat recovery using CFD and CCD techniques, Int. Commun. Heat Mass 57 (2014) 254–263.
[23] M. Hatami, D. Song, D. Jing, Optimization of a circular-wavy cavity filled by nanofluid under the natural convection heat transfer condition, Int. J. Heat Mass Transfer 98 (2016).
[24] Z.H. Wang, X.D. Wang, W.M. Yan, Multi-parameters optimization for microchannel heat sink using inverse problem method, Int. J. Heat Mass Transfer 54 (2011) 2811–2819.
[25] D. Susa, M. Lehtonen, H. Nordman, Dynamic thermal modelling of power transformers, IEEE Trans. Power Delivery 20 (2005) 197–204.
[26] Y.L. He, W.Q. Tao, Y. Wang, J.F. Fan, The research progress of heat exchange equipment comprehensive evaluation index, in: Proceedings of the Annual Conference of Chinese Society of Engineering Thermophysics (2011).
[27] S.G. Kandlikar, W.J. Grande, Evolution of microchannel flow passages-thermohydraulic performance and fabrication technology, Heat Transfer Eng. 24 (2003) 3–17.
[28] A. Sakanova, C.K. Chan, J. Zhao, Performance improvements of microchannel heat sink using wavy channel and nanofluids, Int. J. Heat Mass Transfer 89 (2015) 59–74.